Computational Simulations of the Interactions between Acetyl-Coenzyme-A Carboxylase and Clodinafop: Resistance Mechanism Due to Active and Nonactive Site Mutations

Xiao-Lei Zhu,[†] Hao Ge-Fei,[†] Chang-Guo Zhan,*[,‡] and Guang-Fu Yang*[,†]

Key Laboratory of Pesticide & Chemical Biology, Ministry of Education, College of Chemistry, Central China Normal University, Wuhan 430079, P. R. China, and Department of Pharmaceutical Sciences, College of Pharmacy, University of Kentucky, 725 Rose Street, Lexington, Kentucky 40536

Received May 13, 2009

Grass weed populations resistant to acetyl-CoA carboxylase-inhibiting (ACCase; EC 6.4.1.2) herbicides represent a major problem for the sustainable development of modern agriculture. In the present study, extensive computational simulations, including homology modeling, molecular dynamics (MD) simulations, and molecular mechanics-Poisson−Boltzmann surface area (MM/PBSA) calculations, have been carried out to uncover the detailed molecular mechanism of *Alopecurus myosuroides* resistance to clodinafop, a commercial herbicide targeting ACCase. All the computational model and energetic results indicated that W374C, I388N, D425G, and G443A mutations have great effects on the conformational change of the binding pocket and the hydrogen-bonding interactions. The $\pi-\pi$ interaction between ligand and the residue of Phe377 and Tyr161′, playing an important contribution to the binding affinity, were decreased after mutations. In addition, the hydrogen-bonding interactions between clodinafop and the residues (Ile158′ and Ala54′) disappeared or decreased significantly upon mutation. As a result, the mutant-type ACCase has a lower affinity for the inhibitor binding than the wild-type enzyme, which accounts for the molecular basis of herbicidal resistance. The structural and mechanistic insights obtained from the present study will provide a valuable clue for future designing of a promising inhibitor to reduce drug resistance associated with both active and nonactive site mutations.

1. INTRODUCTION

In both eukaryotes and prokaryotes, acetyl-coenzyme A carboxylase (ACCase; EC 6.4.1.2) is a biotinylated enzyme that catalyzes the carboxylation of acetyl-CoA to produce malonyl-CoA, which consists of a two-step reaction: the ATP-dependent carboxylation of the biotin group on the carboxyl carrier domain catalyzed by the biotin-carboxylase and the transfer of the carboxyl group from biotin to acetyl-CoA catalyzed by the carboxyl-transferase (CT domain).[1,2] Importantly, the CT domain of ACCase has been identified as the target of two structurally distinct herbicides, naming aryloxyphenoxypropionates (APPs) and cyclohexanediones (CHDs).[3,4] Because the plastidic ACCase of grass species is susceptible to herbicides whereas that of broadleaf species is structurally different and not susceptible, APPs and CHDs have been widely used in broadleaf crops to selectively control a variety of grass weeds since their introduction to world agriculture in the late 1970s.[5−7]

In addition to its important role in the agricultural chemistry, ACCase has also been identified as a promising target of drug development for the therapeutic treatments such as obesity, type 2 diabetes, and microbial infections.[8−11] Two informs of ACCase, ACCase1 and ACCase2, have been identified in mammals. ACCase1 is a cytosolic enzyme which controls the committed step in the biosynthesis of long-chain fatty acids,[12] whereas ACCase2 is associated with the outer membrane of mitochondria. Malonyl-CoA, the product of ACCase2, is a potent inhibitor of the transport of long-chain acyl-CoAs for oxidation in the mitochondria.[13,14] Mice lacking ACCase2 have elevated fatty acid oxidation and reduced body fat and body weight, indicating the importance of this enzyme for drug discovery.[9,10]

The frequent use of APPs and CHDs has resulted in many grass weed species developing resistance to these herbicides. As a consequence, 35 resistant weed species in 26 countries have been reported so far (see the Web site of herbicidal resistance at www.weedscience.org/in.asp), which represent a major problem for sustainable agriculture. In most cases, resistance is due to mutation of the CT domain of ACCase, making it less sensitive to herbicide inhibition.[15−18] Among the known weed species resistance to herbicides, *Alopecurus myosuroides*, a monocot weed in the Poaceae family, is one of the most extensively studied species.[15] Since the first report about resistant *A. myosuroides* appeared in 1982, some mutant-type (MT) *A. myosuroides* showing resistance to APPs and CHDs were identified. Recently, five amino acid substitutions in the CT domain of *A. myosuroides* have been demonstrated to be associated with weed resistance,[15] such as Ile-1781-Leu, Trp-2027-Cys, Ile-2041-Asn, Asp-2078-Gly, and Gly-2096-Ala (numbered according to the *A. myosuroides* plastid ACCase). However, the molecular mechanism of mutant-type ACCase resistance to APPs and CHDs has not been established because no data are available regarding the three-dimensional (3D) structure of high plant ACCase in complex with APPs or CHDs inhibitors.

* Corresponding author e-mail: gfyang@mail.ccnu.edu.cn.
[†] Central China Normal University.
[‡] University of Kentucky.

10.1021/ci900174d CCC: $40.75
Published on Web 07/13/2009

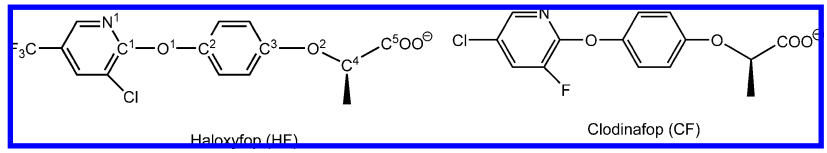

Figure 1. Structures of haloxyfop (HF) and clodinafop (CF).

Table 1. Binding Free Energies (kcal/mol) of the Wild-Type and Mutant Complexes

complex	ΔE_{ele}	ΔE_{VDW}	ΔE_{np}	ΔE_{polar}	ΔE_{bind}	$-T\Delta S$	ΔG_{bind}	$\Delta\Delta G_{bind}$[a]	RF[b]	$\Delta\Delta G_{exp}$[c]
wild-type	46.30 (4.29)[d]	−40.71 (1.87)	−4.96 (0.07)	−20.75 (5.28)	−20.13 (4.96)	7.87	−12.26	---	---	---
G443A	63.71 (5.25)	−43.97 (1.88)	−5.04 (0.06)	−25.25 (6.44)	−10.54 (4.75)	6.10	−4.44	7.82	57.5	2.40
W374C	42.22 (4.57)	−41.61 (2.13)	−4.87 (0.07)	−8.50 (5.08)	−12.76 (4.71)	9.24	−3.52	8.74	90.5	2.67
D425G	24.14 (5.02)	−41.67 (1.82)	−4.71 (0.10)	7.07 (6.00)	−15.17 (4.28)	12.74	−2.43	9.83	125.5	2.87
I388N	52.60 (4.36)	−42.70 (2.33)	−4.95 (0.10)	−14.38 (6.31)	−9.44 (5.06)	6.66	−2.78	9.48	202.5	3.15

[a] $\Delta\Delta G_{bind} = \Delta G_{MT} - \Delta G_{WT}$. [b] $RF = IC_{50,MT}/IC_{50,WT}$, IC_{50} values were taken from ref 15. [c] $\Delta\Delta G_{exp} = RT \ln(IC_{50,MT}/IC_{50,WT}) = 1.366 \log RF$. [d] Standard deviations of averages are shown in parentheses.

Recently, the crystal structures of the CT domain (PDB code: 1OD2, 1OD4) of yeast ACCase and its complex with APPs (PDB code: 1UYR, 1UYS) were determined at 2.7 Å (Å) and 2.5 Å resolution, respectively.[19,20] However, the yeast ACCase is a well-known tolerant to APPs and CHDs. In this study, therefore, various computational techniques, including homology modeling, molecular docking, molecular dynamics (MD) simulations, and the molecular mechanics-Poisson−Boltzmann surface area (MM/PBSA) calculations, were used to construct the 3D structures of the wild-type (WT) and mutant types of CT domain of *A. myosuroides* ACCase and their complex with clodinafop (CF), an APP-type commercial herbicide. Based on the results of computational simulations, the detailed interaction mechanism of the wild-type and mutant *A. myosuroides* ACCase with CF was uncovered. The results indicated that the conformational change of the binding pocket and the hydrogen-bonding network change caused by the residue substitution resulted in the decrease of inhibitor-binding affinity, which is the molecular basis of the resistance mechanism. Our findings will provide a new starting point for the rational design of novel ACCase inhibitors.

2. MATERIALS AND METHODS

Homology Modeling. The sequence of CT domain from *A. myosuroides* was obtained from the Web site of NCBI (Genbank code: AJ310767). The residues from 1654 to 2199 of the CT domain was extracted and then renumbered from 1 to 546. Therefore, according to the new numbering rule, four original mutations of Trp-2027-Cys, Ile-2041-Asn, Asp-2078-Gly, and Gly-2096-Ala selected for the present study allele to W374C, I388N, D425G, and G443A, respectively. Two crystal structures, the free CT domain of yeast ACCase (PDB code 1OD2) and its complex with haloxyfop (HF, as shown in Figure 1) (1UYS), were selected as template for the homology modeling. The CT domain is a dimer; therefore, sequence alignment between AJ310767 and each monomer of 1OD2 (chains A and B) and 1UYS (chains B and C) was performed by using Pairwise_Sequence with default parameters. The results indicated that AJ310767 has 54.8% identity with the monomers of 1OD2 and 52.6% identity with the monomers of 1UYS, respectively. The Modeler 7.0 program implemented in Insight II was used to create the models.[21,22] The homology modeling was performed in two steps. First, one of the two chains of 1OD2 and 1UYS was used to create 100 different monomers of the dimer of free *A. myosuroides* CT and its complex. Then, the other chain of the corresponding CT dimer was used as a template to create another 100 different monomers. To reduce computational time, the Num_Loop_Models was set to 1. The best monomer model was evaluated by their stereochemical quality with the program of PROCHECK (Table 1S in the Supporting Information).[23] Model-16 and model-77 were selected to construct the free CT dimer and model-50 and model-88 for the complex dimer. Finally, to create the CT dimer, we superimposed the selected models to the corresponding monomer in the crystal structures. Then, the dimers of free *A. myosuroides* CT (AM-free) and its complex were obtained using the Merge module in Sybyl 7.1. The residues were renumbered from 1 to 546 for one monomer and from 1′ to 546′ for the other monomer. The inhibitor HF was put into the binding pocket with the coordinate extracted directly from 1UYS.

MD Simulations for *A. myosuroides* CT Domain (AM-Free) and Its Complex with HF (AM-HF). MD simulations were performed to obtain stable structure of the dimer of *A. myosuroides* CT domain. Before MD simulations, quantum chemical calculations were executed for the inhibitors to deduce the atom charges utilized in MD simulations. Geometry optimization was performed, and electrostatic potential was calculated at the HF/6-31G (d) level using the Gaussian 03 program.[24] Atomic charges of the inhibitors were calculated by the RESP fitting method.[25] Partial atomic charge and force-field parameters for the inhibitors were generated by the Antechamber suite.

The general procedure for MD simulations is essentially similar as that used in our previous computational studies.[26−30] Briefly, the MD simulations were performed using the Sander module of the AMBER 8.0 simulation package. Force-field parameters and partial charges for the protein come from the Parm99 force field.[31,32] Both systems were neutralized by adding Na^+ and then solvated in an octahedral box of TIP3P water molecules,[33] which extended at least 5 Å from any given protein atom for AM-free and AM-HF complex. The solvated systems were optimized prior to the MD simulations. In the first stage, the protein was fixed with a constraint of 500 kcal/mol/Å^2 and just minimized the positions of water molecules and Na^+ ions for 3000 steps. In the second stage, the entire system was minimized for 500 steps steepest descent (SD) and 5500 steps conjugate

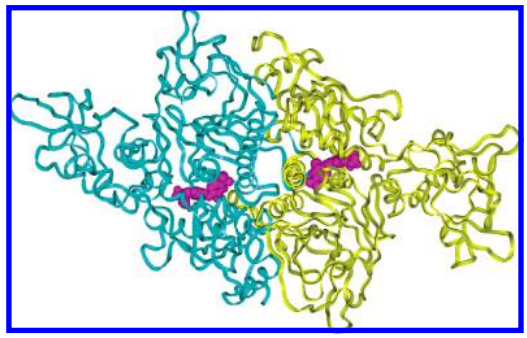

Figure 2. The ribbon structure of the AM-CF complex. CF molecules in magenta adopted almost the same conformations in the two symmetric binding pockets. The left binging pocket (blue) was fixed during the MD simulations.

gradient (CG). After full relaxation and the entire solvated systems were subjected for further energy-minimized, both systems were slowly heated from $T = 10$ K to $T = 300$ K in 100 ps for the AM-free and 30 ps for the AM-HF complex, respectively. In order to avoid the two monomers appearing translation, a 100 kcal/mol/Å^2 harmonic force constant was set for the protein and inhibitor. For the AM-HF complex, the additional 30 ps MD simulations in 300 K were carried out with restriction. Subsequently, 1400 ps and 1200 ps MD simulations for AM-free and AM-HF complex were performed without any restriction.

The MD simulations were performed with a periodic boundary condition in an NPT ensemble at $T = 300$ K with Berendsen temperature coupling[34] and constant pressure ($P = 1$ atm) with isotropic molecule-based scaling.[24] The SHAKE algorithm[35] was used to fix all covalent bonds containing hydrogen atom, and a time step of 2 fs was used. The pressure was adjusted by isotropic position scaling. The particle mesh Ewald (PME) method[36,37] was used to treat long-range electrostatic interactions. A residue-based cutoff of 10 Å was utilized for noncovalent interactions. During the MD simulations, the coordinates of the simulated systems were saved every 1 ps.

MD Simulations for the *A. myosuroides* CT Domain and Its Mutants in Complex with Clodinafop (CF). As shown in Figure 1, CF has a very similar chemical structure to HF. So, the starting structure of the WT *A. myosuroides* CT-CF complex (AM-CF) was obtained by direct modification of the substituents of HF in the structure of the AM-HF complex. This method was proved to be useful in studying the binding model of inhibitors with the same chemical scaffold.[38−40]

As shown in Figure 2, there are two symmetric binding pockets in the 3D structures of AM-CF complex and its mutants. Hence, only one binding pocket was subjected to perform MD simulations to save computational cost. The structure of the AM-CF complex and its mutants were solvated by a 50 Å cap of TIP3P water centered on the inhibitor and then neutralized by adding Na^+. The starting structures of W374C, I388N, D425G, and G443A mutant complexes were obtained by the direct mutation of the corresponding residues of the MD-equilibrium wild-type AM-CF complex using the biopolymer module in Sybyl 7.1. During the MD simulations of mutant complexes, the important H-bonds between CF and the protein was fixed in the first 60 ps and then opened.

Binding Free Energy Calculation (MM/PBSA). The binding free energies were calculated by using the molecular mechanics-Poisson−Boltzmann surface area (MM/PBSA) binding free energy calculation method.[41,42] In the MM/PBSA method, the free energy of the receptor/protein-inhibitor binding, ΔG_{bind}, is obtained from the difference between the free energies of the receptor/ protein−ligand complex (G_{cpx}) and the unbound receptor/protein (G_{rec}) and ligand (G_{lig}) as follows

$$\Delta G_{bind} = G_{cpx} - (G_{rec} + G_{lig}) \quad (1)$$

The binding free energy (ΔG_{bind}) was evaluated as a sum of the changes in the molecular mechanical (MM) gas-phase binding energy (ΔE_{MM}), solvation free energy (ΔG_{sol}), and entropic contribution ($-T\Delta S$)

$$\Delta G_{bind} = \Delta E_{bind} - T\Delta S \quad (2)$$

$$\Delta E_{bind} = \Delta E_{MM} + \Delta G_{sol} \quad (3)$$

ΔE_{MM} was calculated by using the following equation

$$\Delta E_{MM} = \Delta E_{ele} + \Delta E_{vdw} \quad (4)$$

where ΔE_{ele} and ΔE_{vdw} are electrostatic and van der Waals interaction energies, respectively, between a ligand and a protein. These energies were computed using the same parameter set as that used in the MD simulation. The solvation free energy ΔG_{sol} consists of two parts[43]

$$\Delta G_{sol} = \Delta G_{PB} + \Delta G_{np} \quad (5)$$

The electrostatic contribution to the solvation free energy (ΔG_{PB}) was calculated by the Poisson−Boltzmann (PB) method using the MM-PBSA module of the AMBER 8 program.[32] ΔG_{np} is the nonelectrostatic contribution to the solvation free energy determined as a function of the solvent accessible surface area (SA).[44,45] Therefore, ΔG_{np} was estimated using a simple empirical relation of $\Delta G_{np} = \gamma SA + b$ ($\gamma = 0.00542$ kcal·mol^{-1}·Å^{-2}, $b = 0.92$ kcal·mol^{-1}), where SA is determined with the LCPO method as implemented in AMBER 8.0. The inteior and exterior dielectric constants were set to 1 and 80, respectively. The grid spacing was set to $^2/_3$ Å. In the first protocol, the structures of protein, ligand, and their complex were taken from the same MD trajectory, stripped of all water molecules, Na^+ ions. Then, all energy components and binding free energy were calculated for all three molecules generated from the 100 snapshots. For wild-type and mutant complexes, the intervals were set to 1 ps during the last 100 ps simulations.

Further, the entropic contribution to the binding free energy can be divided into two parts: the solvation entropy change (ΔS_{sol}) and the conformational entropy change (ΔS_{conf}). The detailed computational procedure used to evaluate the entropic contribution ($-T\Delta S$) to the binding free energy was the same as that described in our recent publications.[46−48]

3. RESULTS AND DISCUSSION

Structures of Wild-Type *A. myosuroides* CT Dimer and Its Complex with HF. The crystal structure of yeast CT is a dimer and has two symmetric binding pockets at the interface of two monomers. Interestingly, however, there is no corresponding binding pocket in the crystal structure of free yeast CT domain. Upon the inhibitor binding, residue

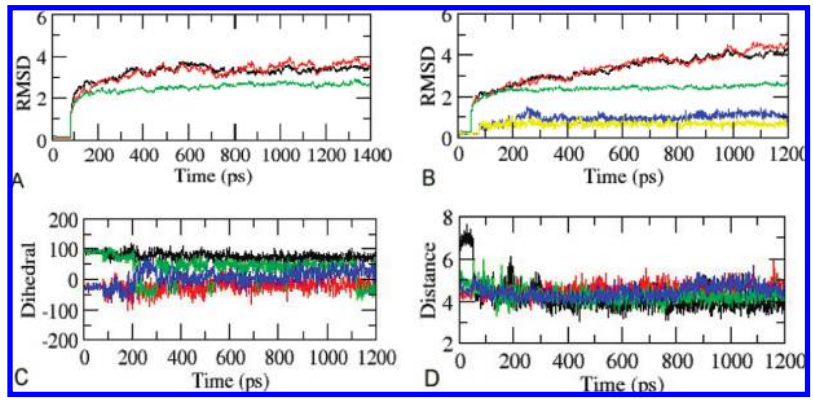

Figure 3. Plots of the rmsd of wild-type AM-free (A) and AM-HF (B) vs the simulation time. The black and red lines represent the rmsd of backbone atoms in two monomers, respectively. The green line represents the rmsd of backbone atoms of the protein except for the end terminal of each monomer (the residues 57−122, 448−516, 56′−124′, and 453′−516′). The blue and yellow lines represent the rmsd of heavy atoms of HF in the left and right pocket, respectively. (C) Variability of the dihedral angle of N1−C1−O1−C2 and C3−O2−C4−C5 in HF vs simulation time. The green and blue lines represent HF-L in the left pocket. The black and red lines represent HF-R in the right pocket. (D) Some key distances in AM-HF vs the simulation time. Black and red lines represent the distance between the centroid of pyridyl ring of HF-R and the center of benzene ring of Phe377 and Tyr161′ in the right pocket, respectively. Green and blue lines represent the distance between the center of pyridyl ring of HF-L and the centroid of benzene ring of Phe377′ and Tyr161 in the left pocket, respectively.

Phe377, allele to Phe1956′ in the crystal structure, took significant conformational change by rotating about 120° to form the binding pocket.[19,20] Hence, two forms of wild-type *A. myosuroides* CT domain were modeled in the present study: free CT domain (AM-free) and its complex with HF (AM-HF).

The Root-Mean-Square Displacement (rmsd) values for the MD simulations were plotted in Figure 3A,B. The rmsd plots indicated that the systems of AM-free and AM-HF achieved equilibrium very quickly. At the same time, we also examine the dihedral angle change of the inhibitor in the AM-HF complex as shown in Figure 3C and the distance change between the centroid of the pyridyl ring of HF and the phenyl ring of Phe377 and Tyr161′ which formed $\pi-\pi$ interactions with the inhibitor as shown in Figure 3D. The rmsd plots of the backbone atoms and some key distances indicated that the system of AM-free and AM-HF complex have achieved equilibrium after MD simulations.

The average MD-simulated structure of AM-HF was shown in Figure 4. Similar to the crystal structure of yeast CT dimer in complex with HF, there are two symmetric binding pockets in the MD-equilibrated AM-HF complex. For convenience, the left and right pockets are called L-pocket and R-pocket, respectively. Originally, there is no binding pocket in the free CT dimer. Upon the inhibitor binding, taking the R-pocket as an example, Phe377 and Tyr161′ as shown in Figure 4A experienced significant conformation changes by rotating respectively about 100° and 30° to accommodate the inhibitor. Meanwhile, the residues of Phe377, Tyr161′, Trp374, Trp346, Ile158′, and Ala54′ translated about 0.5−3.3 Å. Finally, inhibitor HF was sandwiched by Phe377 and Tyr161′ *via* $\pi-\pi$ interactions and formed an important H-bond interaction with Ile158′. These key interactions can also be found in the crystal structure of yeast CT dimer in complex with HF.

In addition, we calculated the binding free energies of HF in the left and right binding pocket by the MM/PBSA method. The results (Table 2S, Supporting Information) indicated that the binding free energies (ΔG_{bind}) of HF are −11.62 and −15.22 kcal/mol for the L-pocket and R-pocket,

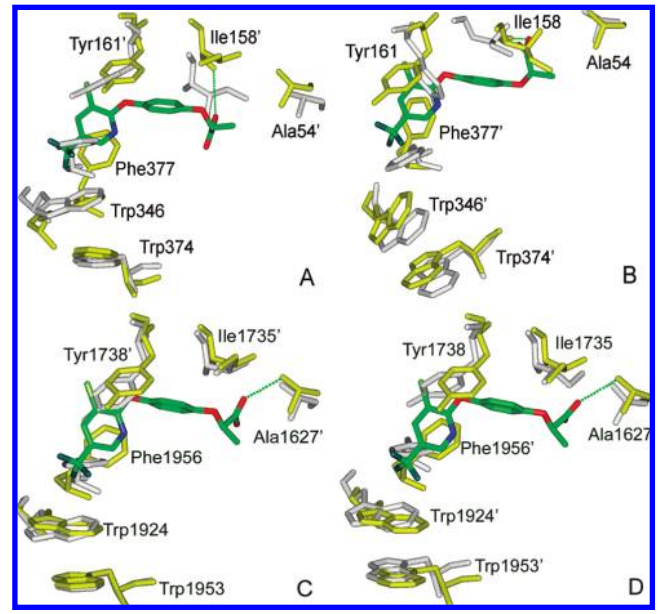

Figure 4. (A) The superposition of the key residues of the right binding pocket (R-pocket) of the AM-HF complex (green and yellow) with that of AM-free (gray) after MD. (B) The superposition of the key residues of the left binding pocket (L-pocket) of the AM-HF complex (green and yellow) with that of AM-free (gray). (C) The superposition of the key residues of the right binding pocket of 1UYS (green and yellow) with 1OD2 (gray). (D) The superposition of the key residues of the left binding pocket of 1UYS (green and yellow) with 1OD2 (gray).

respectively. For comparison, we also calculated the binding energy of the crystal structure of the HF-complexed yeast CT. The ΔE_{bind} of HF are −13.88 and −16.36 kcal/mol for the L-pocket and R-pocket. Theoretically speaking, the inhibitor should have the same binding free energy for the symmetric binding pocket. However, it is well-known that the result of the MM/PBSA calculation is sensitive to the small conformational difference. Therefore, it is understandable that HF have different binding free energies in the two binding pockets. Because the right binding pockets gave a lower binding free energy, we selected the R-pocket for the next calculation in order to reduce the simulation time.

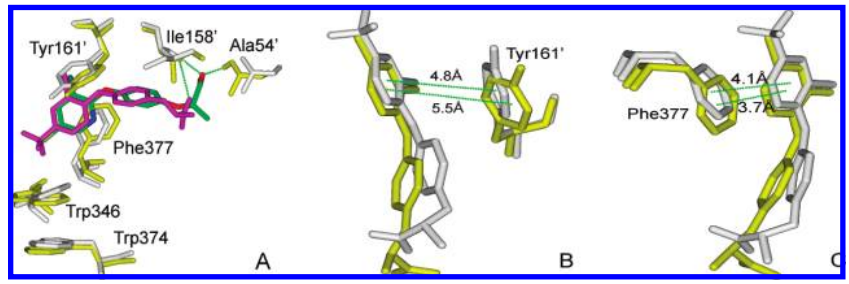

Figure 5. (A) The superposition of the key residues of the right binding pocket (R-pocket) of the AM-CF complex (green and yellow) with that of AM-HF (gray and magenta) after MD. (B) The distance between the phenyl ring centroid of Tyr161′ with the pyridyl ring centroid of CF (yellow) and HF (gray). (C) The distance between the phenyl ring centroid of Phe377 with the pyridyl ring centroid of CF (yellow) and HF (gray).

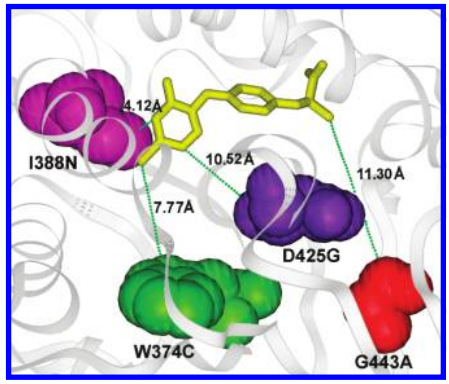

Figure 6. Relative locations of W374C (green), I388N (magenta), D425G (purple), and G443A (red) mutations.

Structures of *A. myosuroides* CT Dimer in Complex with CF. The same procedure used to construct the 3D structure of the AM-HF complex was extended to construct the equilibrated 3D structure of the AM-CF complex. As shown in Figure 5A, the pyridyl ring of CF was also sandwiched by Phe377 and Tyr161′ *via* $\pi-\pi$ interactions. As shown in Figure 5B,C, the distance between the pyridyl ring centroid of CF and the phenyl ring centroid of Tyr161′ and Phe377 are 5.5 and 3.7 Å, respectively. The corresponding distances in the AM-HF complex are 4.8 and 4.1 Å. Therefore, HF has stronger *van der Waals* interactions (−11.07 kcal/mol) with these two residues than CF (−9.67 kcal/mol), which might account for the lower activity of CF (IC_{50} = 4.0 nM) than HF (IC_{50} = 1.4 nM). In addition, the carboxyl oxygen atom of CF formed two H-bonds with Ile158′ and Ala54′, respectively. If only the R-pocket was considered, the calculated binding free energies for CF and HF are −12.26 kcal/mol and −15.22 kcal/mol, which is qualitatively consistent with the experimental order of IC_{50} values. These results indicated that the computational protocols used herein are reliable.

Structural Comparison of the Wild-Type and Mutant AM-CF Complexes. Mutations W374C, I388N, and D425G belong to the substitution of the larger groups with the smaller one. Although mutation G443A belongs to the substitution of the smaller group with the larger one, its location is a nonactive site. The relative location of these four mutation sites was shown in Figure 6. Therefore, these mutations are not expected to dramatically influence the protein folding. So, the starting structures of the four mutant AM-CF complexes were obtained by direct substitution of the corresponding residues of the wild-type AM-CF complex and then subjected to MD simulations (Figure 2S, Supporting Information).

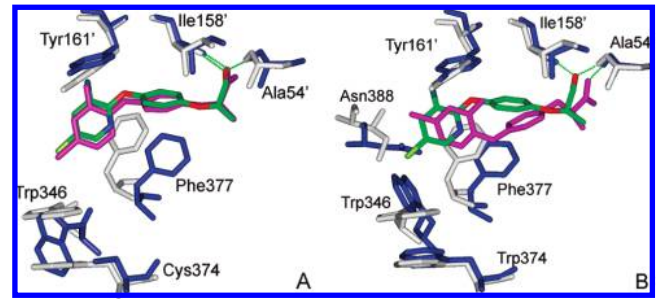

Figure 7. The overlay between the structure of wild-type AM-CF and the structure of the W374C mutant complex (A) and the I388N mutant complex (B) after MD. The wild-type AM-CF complex was colored by gray and green. W374C and I388N mutant complexes were colored by magenta and blue.

To clarify the effects of mutations W374C, I388N, D425G, and G443A on the conformations of the binding pocket, the average MD-simulated structure of each mutant complex was superimposed with that of the wild-type AM-CF complex based on the backbone atoms in the R-pocket. The results indicated that Trp346 and Phe377 in these complexes always displayed significant conformational changes upon mutation, which resulted in the decrease of $\pi-\pi$ interaction energy between the protein and CF. At the same time, the hydrogen bonding network also changed, and some important H-bonds disappeared or weakened sharply after mutation.

Taking the W374C mutant complex as an example, as shown in Figure 7A, there is an important $\pi-\pi$ interaction between the side indole rings of Trp346 and Trp374 in the wild-type complex, which disappeared after W374C mutation. As a result, the indole ring of Trp346 rotated about 60° upon mutation. Meanwhile, the centroid of Phe377 translated toward the right about 2.70 Å. The distance between the carboxyl oxygen atom of CF and the H atom of backbone HN groups of Ile158′ and Ala54′ was changed from 2.07 Å to 1.96 Å and from 2.01 Å to 1.95 Å, respectively. For the I388N mutant complex as shown in Figure 7B, the indole ring of Trp346 rotated about 100° and the centroid of Phe377 translated toward the right about 2.11 Å upon mutation. Interestingly, the conformation of CF is highly conserved upon W374C mutation. On the contrary, CF experienced significant conformational change upon I388N mutation. The distance between the carboxyl oxygen atom of CF and the H atom of backbone HN groups of Ile158′ and Ala54′ was changed to 3.37 Å and 1.83 Å, respectively. As shown in Figure 8, the indole ring of Trp346 rotated about 100° and the centroid of Phe377 translated toward the right about 2.30 Å after D425G mutation. Meanwhile, the centroid of CF also translated toward the

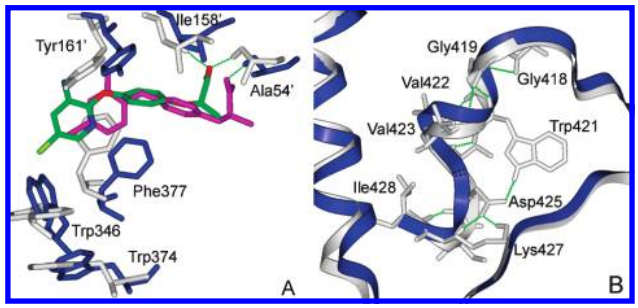

Figure 8. The overlay of R-pocket (A) and the neighborhood residues around D425G (B) between the structure of wild-type AM-CF and the structure of the D425G mutant complex after MD. The wild-type complex was colored by gray and green. The D425G mutant complex was colored by magenta and blue. The green dot line represents H-bonds in the wild-type complex.

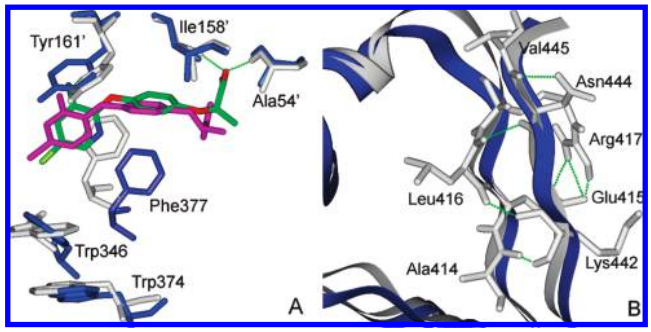

Figure 9. The overlay of R-pocket (A) and the neighborhood residues around G443A (B) between the structure of wild-type AM-CF and the structure of the G443A mutant complex after MD. The wild-type complex was colored by gray and green. The G443A mutant complex was colored by magenta and blue. The green dot line represents H-bonds in the wild-type complex.

right about 2.25 Å. As a result, the two corresponding hydrogen-bonding distances were changed to 3.46 Å and 1.80 Å, respectively. For the G443A mutant complex as shown in Figure 9, the indole ring of Trp346 rotated about 20° and the centroid of Phe377 translated toward the right about 3.04 Å. The two corresponding hydrogen-bonding distances were changed to 4.29 Å and 4.73 Å, respectively. In general, the conformation of CF is relatively conserved upon G443A mutation.

It should be noted additionally as to why the nonactive site mutations such as D425G and G443A resulted in significant conformational changes of Trp346 and Phe377. As shown in Figures 8B and 9B, D425G mutation resulted in the break of the H-bond network between D425 and K427, D425 and W421, D425 and I428, V422 and G419, and G419 and G418, while the G443A mutation resulted in the break of the H-bond network A414 and K442, E415 and R417, L416 and K442, K442 and A414, and V445 and N444. As a consequence, the conformation of the binding pocket would take a corresponding change to accommodate the inhibitor binding.

Binding Free Energies Changes and Drug Resistance. The influence of mutations on the binding free energy (ΔG_{bind}) was examined for each modeled complex structure. Summarized in Table 1 are the results obtained from the MM/PBSA calculations for the wild-type and mutant AM-CF complexes. As seen in Table 1, the binding energy (ΔE_{bind}, neglecting the entropic contribution) calculated for the wild-type AM-CF complex is −20.13 kcal/mol. However, the ΔE_{bind} values calculated for the mutant AM-CF complexes range from −9.44 to −15.17 kcal/mol, with the lowest ΔE_{bind} value corresponding to the D425G mutant and the highest ΔE_{bind} value corresponding to the I388N mutant. Compared with the calculated entropic contributions ($-T\Delta S$) for the wild-type AM-CF complex, W374C and D425G mutations experienced entropic increase, while G443A and I388N mutations experienced entropic loss. Therefore, the Gibbs binding free energies (ΔG_{bind}) calculated for the wild-type and mutant AM-CF complexes range from −2.43 to −12.26 kcal/mol.

The relative binding free energy shifts ($\Delta\Delta G_{bind}$) from the wild-type to the mutant complex calculated can be used to qualitatively predict the drug resistance levels for CF due to the mutations (W374C, I388N, D425G, and G443A). According to the calculated $\Delta\Delta G_{bind}$ values summarized in Table 1, all these mutations should cause the drug resistance for CF, and the highest resistance level should be associated with D425G mutation. It is important to compare our computational results with available experimental data. In order to eliminate error, the reported experimental data (IC_{50}) were translated to resistance factor ($RF = IC_{50,MT}/IC_{50,WT}$). Although the experimental IC_{50} values should not be compared quantitatively with the calculated enzyme−inhibitor binding affinities, it is reasonable to assume that the RF are usually (although not generally) consistent with the relative binding free energies ($\Delta\Delta G_{bind} = \Delta G_{MT} - \Delta G_{WT}$) of the inhibitor with the wild-type and mutant enzyme. As shown in Table 1, except for I388N and D425G, the calculated $\Delta\Delta G_{bind}$ values are consistent with the RF. In addition, there is a good linear correlation ($r^2 = 0.74$) between the calculated $\Delta\Delta G_{bind}$ values and the $\Delta\Delta G_{exp}$ values derived from the experimental resistance data ($\Delta\Delta G_{exp} = RT \ln RF = 1.366 \log RF$), suggesting that the drug resistance due to the residue mutation is mainly attributed to the decrease in the binding affinity for the inhibitor.

4. CONCLUSION

In summary, the mechanism of resistance due to W374C, I388N, D425G, and G443A mutations has been uncovered through extensive computational simulations. Mutations W374C and I388N are active sites, while D425G and G443A, having no direct contact with the inhibitor, are nonactive sites. In addition, W374C, I388N, and D425G belong to the substitution of the larger groups with the smaller one, but G443A belongs to the substitution of the smaller group with the larger one. The computational simulations demonstrated that W374C, I388N, D425G, and G443A mutations all have great effects on the conformational change of the binding pocket and the hydrogen-bonding interactions. The $\pi-\pi$ interaction between ligand and the residue of Phe377 and Tyr161′, playing an important contribution to the binding affinity, were decreased after mutations. In addition, the hydrogen-bonding interactions between clodinafop and the residues (Ile158′ and Ala54′) disappeared or decreased significantly upon mutation. As a result, the mutant-type CT has a lower affinity for the inhibitor binding than the wild-type CT, which is the molecular basis of herbicidal resistance. The structural and mechanistic insights obtained from the present study will provide a valuable clue for future designing of a promising

inhibitor to reduce drug resistance associated with both active and nonactive site mutations.

ACKNOWLEDGMENT

The present work was supported in part by national NSFC grants and the national 973 Program (2003CB114400).

Supporting Information Available: Materials about the results of PROCHECK, the binding free energies for HF, the distance between the H-bond acceptor and the H-bond donor for AM-CF and its mutant complexes, the rmsd for AM-HF, the rmsd for AM-CF and its mutant complexes, the VDW interaction for AM-CF, the key residues conformation in 1OD2 and AM-free, the binding model HF with CT in two binding pockets, and the binding model AM-CF. This material is available free of charge via the Internet at http://pubs.acs.org.

REFERENCES AND NOTES

(1) Nikolau, B. J.; Ohlrogge, J. B.; Wurtele, E. S. Plant biotin-containing carboxylases. *Arch. Biochem. Biophys.* **2003**, *414*, 211–222.
(2) Egli, M. A.; Gengenbach, B. G.; Gronwald, J. W.; Somers, D. A.; Wyse, D. L. Characterization of maize acetyl-coenzyme A carboxylase. *Plant. Physiol.* **1993**, *101*, 499–506.
(3) Rendina, A. R.; Craig-Kennard, A. C.; Beaudoin, J. D.; Breen, M. K. Inhibition of acetyl-coenzyme A carboxylase by two classes of grass-selective herbicides. *J. Agric. Food Chem.* **1990**, *38*, 1282–1287.
(4) Burton, J. D.; Gronwald, J. W.; Keith, R. A.; Somers, D. A.; Gegenbach, B. G.; Wyse, D. L. Kinetics of inhibition of acetyl-coenzyme A carboxylase by sethoxydim and haloxyfop. *Pestic. Biochem. Physiol.* **1991**, *39*, 100–109.
(5) Sasaki, Y.; Konishi, T.; Nagano, Y. The compartmentation of acetyl-coenzyme A carboxylase in pants. *Plant. Physiol.* **1995**, *108*, 445–449.
(6) Post-Beittenmiller, D. Biochemistry and molecular biology of wax production in plants. *Annu. Rev. Plant. Physiol. Plant. Mol. Biol.* **1996**, *47*, 405–430.
(7) Konishi, T.; Shinohara, K.; Yamada, K.; Sasaki, Y. Acetyl-CoA carboxylase in higher plants: most plants other than gramineae have both the prokaryotic and eukaryotic forms of this enzyme. *Plant. Cell. Phusiol.* **1996**, *37*, 117–122.
(8) Campbell, J. W.; Cronan, J. J. E. BACTERIAL FATTY ACID BIOSYNTHESIS: Targets for Antibacterial Drug Discovery. *Annu. Rev. Microbiol.* **2001**, *55*, 305–332.
(9) Abu-Elheiga, L.; Matzuk, M. M.; K. Abo-Hashema, A. H.; Wakil, S. J. Continuous Fatty Acid Oxidation and Reduced Fat Storage in Mice Lacking Acetyl-CoA Carboxylase 2. *Science* **2001**, *291*, 2613–2616.
(10) Lenhard, J. M.; Gottschalk, W. K. Preclinical developments in type 2 diabetes. *Adv. Drug Delivery Rev.* **2002**, *54*, 1199–1212.
(11) Levert, K. L.; Waldrop, G. L.; Stephens, J. M. A Biotin Analog Inhibits Acetyl-CoA Carboxylase Activity and Adipogenesis. *J. Biol. Chem.* **2002**, *277*, 16347–16350.
(12) Wakil, S. J.; Stoops, J. K.; Joshi, V. C. Fatty Acid Synthesis and its Regulation. *Annu. Rev. Biochem.* **1983**, *52*, 537–579.
(13) McGarry, J. D.; Brown, N. F. The Mitochondrial Carnitine Palmitoyltransferase System- From Concept to Molecular Analysis. *Eur. J. Biochem.* **1997**, *244*, 1–14.
(14) Ramsay, R. R.; Gandour, R. D.; Van der Leij, F. R. Molecular enzymology of carnitine transfer and transport. *Biochim. Biophys. Acta* **2001**, *1546*, 21–43.
(15) Délye, C.; Zhang, X. Q.; Michel, S.; Matejicek, A.; Powles, S. B. Molecular bases for sensitivity to acetyl-coenzyme a carboxylase inhibitors in black-grass. *Plant Physiol.* **2005**, *137*, 794–806.
(16) Liu, W. J.; Harrison, D. K.; Chalupska, D.; Gornicki, P.; O'Donnell, C. C.; Adkins, S. W.; Haselkorn, R.; Williams, R. R. Single-site mutations in the carboxyltransferase domain of plastid acetyl-CoA carboxylase confer resistance to grass-specific herbicides. *Proc. Natl. Acad. Sci. U.S.A.* **2007**, *104*, 3627–3632.
(17) Yu, Q.; Collavo, C.; Zheng, M. Q.; Owen, M.; Sattin, M.; Powles, S. Diversity of ACCase mutations in resistant Lolium populations: Evaluation using clethodim. *Plant. Physiol.* **2007**, *145*, 547–558.
(18) Délye, C. Weed resistance to acetyl coenzyme A carboxylase inhibitors: an update. *Weed Sci.* **2005**, *53*, 728–746.
(19) Zhang, H.; Yang, Z. R.; Shen, Y.; Tong, L. Crystal structure of the carboxylase domain of acetyl coenzyme-A carboxylase. *Science* **2003**, *299*, 2064–2067.
(20) Zhang, H.; Tweet, B.; Tong, L. Molecular basis for the inhibiton of the carboxyltransferase domain of acetyl coenzyme-A carboxylase by haloxyfop and diclofop. *Proc. Natl. Acad. Sci. U.S.A.* **2004**, *101*, 5910–5915.
(21) Sali, A.; Blundell, T. L. Comparative protein modelling by satisfaction of spatial restraints. *J. Mol. Biol.* **1993**, *234*, 779–815.
(22) Sali, A.; Overington, J. P. Derivation of rules for comparative protein modeling from a database of protein structure alignments. *Protien Sci.* **1994**, *3*, 1582–1596.
(23) Laskowski, R. A.; MacArthur, M. W.; Moss, D. S.; Thornton, J. M. PROCHECK: a program to check the stereochemical quality of protein structures. *J. Appl. Crystallogr.* **1993**, *26*, 283–291.
(24) Frisch, M. J.; Trucks, G. W.; Schlegel, H. B.; Scuseria, G. E.; Robb, M. A.; Cheeseman, J. R.; Montgomery, J. A., Jr.; Verven, T.; Kudin, K. N.; Burant, J. C.; Millam, J. M.; Iyengar, S. S.; Tomasi, J.; Barone, V.; Mennucci, B.; Cossi, M.; Scalmani, G.; Rega, N.; Petersson, G. A.; Nakatsuji, H.; Hada, M.; Ehara, M.; Toyota, K.; Fukuda, R.; Hasegawa, J.; Ishida, M.; Nakajima, T.; Honda, Y.; Kitao, O.; Nakai, H.; Klene, M.; Li, X.; Knox, J. E.; Hratchian, H. P.; Cross, J. B.; Adamo, C.; Jaramillo, J.; Gomperts, R.; Stratmann, R. E.; Yazyev, O.; Austin, A. J.; Cammi, R.; Pomelli, C.; Ochterski, J. W.; Ayala, P. Y.; Morokumo, K.; Voth, G. A.; Salvador, P.; Dannenberg, J. J.; Zakrzewski, V. G.; Dapprich, S.; Daniels, A. D.; Strain, M. C.; Farkas, O.; Malick, D. K.; Rabuck, A. D.; Raghavachari, K.; Foresman, J. B.; Ortiz, J. V.; Cui, Q.; Baboul, A. G.; Clifford, S.; Cioslowski, J.; Stefanov, B. B.; Liu, G.; Liashenko, A.; Piskorz, P.; Komaromi, I.; Martin, R. L.; Fox, D. J.; Keith, T.; Al-Laham, M. A.; Peng, C. Y.; Nanayakkara, A.; Challacombe, M.; Gill, P. M.; Wong, M. W.; Gonzalez, C.; Pople, J. A. *Gaussian 03, revision A.1*; Gaussian, Inc.: Pittsburgh, 2003.
(25) Cornell, W. D.; Cieplak, P.; Bayly, C. I.; Kollmann, P. A. Application of RESP charges to calculate conformational energies, hydrogen bond energies, and free energies of solvation. *J. Am. Chem. Soc.* **1993**, *115*, 9620–9631.
(26) Zhu., X. L.; Zhang., L.; Chen., Q.; Wan,., J.; Yang., G. F. Interactions of Aryloxyphen- oxypropionic Acids with Sensitive and Resistant Acetyl-Coenzyme A Carboxylase by Homology Modeling and Molecular Dynamic Simulations. *J. Chem. Inf. Model.* **2006**, *46*, 1819–1826.
(27) Gao, D. Q.; Cho, H.; Yang, W. C.; Pan, Y. M.; Yang, G. F.; Tai, H. H.; Zhan, C. G. Computational design of a human butyrylcholinesterase mutant for accelerating cocaine hydrolysis based on the transition-state simulation. *Angew. Chem., Int. Ed.* **2006**, *45*, 653–657.
(28) Pan, Y. M.; Gao, D. Q.; Yang, W. C.; Cho, H.; Yang, G. F.; Tai, H. H.; Zhan, C. G. Computational Redesign of Human Butyrylcholinesterase for Anti-Cocaine Medication. *Proc. Natl. Acad. Sci. U.S.A.* **2005**, *102*, 16656–16661.
(29) AbdulHameed, M. D. M.; Hamza, A.; Zhan, C. G. Microscopic modes and free energies of 3-phosphoinositide-dependent kinase-1 (PDK1) binding with celecoxib and other inhibitors. *J. Phys. Chem. B* **2006**, *110*, 26365–26374.
(30) Hamza, A.; Cho, H.; Tai, H. H.; Zhan, C. G. Molecular dynamics simulation of cocaine binding with human butyrylcholinesterase and its mutants. *J. Phys. Chem. B* **2005**, *109*, 4776–4782.
(31) Hornak, V.; Abel, R.; Okur, A.; Strockbine, B.; Roitberg, A.; Simmerling, C. Comparison of multiple Amber force fields and development of improved protein backbone parameters. *Proteins* **2006**, *65*, 712–725.
(32) Case, D. A.; Darden, T.; Cheatham, T. E., III; Simmerling, C.; Wang, J.; Duke, R. E.; Luo, R. *AMBER8 Users' Manaual*; University of California, 2004.
(33) Jorgensen, W. L.; Chandrasekhar, J.; Madura, J. D. Comparison of simple potential functions for simulating liquid water. *J. Chem. Phys.* **1983**, *79*, 926–935.
(34) Berendsen, H. C.; Postma, J. P. M.; van Gunsteren, W. F.; DiNola, A.; Haak, J. R. Molecular dynamics with coupling to an external bath. *J. Chem. Phys.* **1984**, *81*, 3684–3690.
(35) Ryckaert, J. P.; Ciccotti, G.; Berendsen, H. J. C. Numerical integration of the cartesian equations of motion of a system with constraints: molecular dynamics of n-alkanes. *J. Comput. Phys.* **1977**, *23*, 327–341.
(36) Darden, T.; York, D.; Pedersen, L. Particle mesh Ewald: An N·log (N) method for Ewald sums in large systems. *J. Chem. Phys.* **1993**, *98*, 10089–10092.
(37) Essmann, U.; Perera, L.; Berkowitz, M. L. A smooth particle mesh Ewald method. *J. Chem. Phys.* **1995**, *103*, 8577–8593.
(38) Rafi, S. B.; Cui, G. L.; Song, K.; Cheng, X. L.; Tonge, P. J.; Simmerling, C. Insight through Molecular Mechanics Poisson-Boltzmann Surface Area Calculations into the Binding Affinity of Triclosan

and Three Analogues for FabI, the E. coli Enoyl Reductase. *J. Med. Chem.* **2006**, *49*4574–4580.
(39) Hou, T. J.; Yu, R. Molecular Dynamics and Free Energy Studies on the Wild-type and Double Mutant HIV-1 Protease Complexed with Amprenavir and Two Amprenavir-Related Inhibitors: Mechanism for Binding and Drug Resistance. *J. Med. Chem.* **2007**, *50*, 1177–1188.
(40) Weis, A.; Katebzadeh, K.; Söderhjelm, P.; Nilsson, I.; Ryde, U. Ligand Affinities Predicted with the MM/PBSA Method: Dependence on the Simulation Method and the Force Field. *J. Med. Chem.* **2006**, *49*, 6596–6606.
(41) Wu, E. L.; Mei, Y.; Han, K. L.; Zhang, Z. H. J. Quantum and Molecular Dynamics Study for Binding of Macrocyclic Inhibitors to Human a-Thrombin. *Biophys. J.* **2007**, *92*, 4244–4253.
(42) Wu, E. L.; Han, K. L.; Zhang, Z. H. J. Selectivity of Neutral/Weakly Basic P1 Group Inhibitors of Thrombin and Trypsin by a Molecular Dynamics Study. *Chem.--Eur. J.* **2008**, *14*, 8704–8714.
(43) Bardi, J. S.; Luque, I.; Freire, E. Structure-based thermodynamic analysis of HIV-1 protease inhibitors. *Biochemistry* **1997**, *36*, 6588–6596.
(44) Sitkoff, D.; Sharp, K. A.; Honig, B. Accurate Calculation of Hydration Free Energies Using Macroscopic Solvent Models. *J. Phys. Chem.* **1994**, *98*, 1978–1988.
(45) Connolly, M. L. Analytical molecular surface calculation. *J. Appl. Crystallogr.* **1983**, *16*, 548–558.
(46) Hao, G. F.; Zhu, X. L.; Ji, F. Q.; Zhang, L.; Yang, G. G.; Zhan, C. G. Understanding the Mechanism of Drug Resistance Due to a Codon Deletion in Protoporphyrinogen Oxidase through Computational Modeling. *J. Phys. Chem. B* **2009**, *113*, 4865–4875.
(47) Ji, F. Q.; Niu, C. W.; Chen, C. N.; Chen, Q.; Yang, G. F.; Xi, Z.; Zhan, C. G. Computational Design and Discovery of Conformationally Flexible Inhibitors of Acetohydroxyacid Synthase to Overcome Drug Resistance Associated with the W586L Mutation. *ChemMedChem.* **2008**, *3*, 1203–1206.
(48) Pan, Y. M.; Gao, D. Q.; Zhan, C. G. Modeling the Catalysis of Anti-Cocaine Catalytic Antibody: Competing Reaction Pathways and Free Energy Barriers. *J. Am. Chem. Soc.* **2008**, *130*, 5140–5149.

CI900174D